PLANETARY SCIENCE INSTITUTE

LUNAR RADAR BACKSCATTER STUDIES

—

FINAL REPORT

—

NASW 3205

5-420-71-780-09

19 October 1979

Prepared by

Thomas W. Thompson
Principal Investigator
Planetary Science Institute
Pasadena, CA 91101

INDEX

OVERVIEW

A proposal entitled "Lunar Radar Backscatter Studies" was submitted to the NASA Lunar and Planetary Program in August 1977, accepted by the reviewers, and funded for the period of 15 July 1978 - 14 October 1978.

The Statement of Work for this grant states the contractor will accomplish the following:

(a) Characterize lunar surface material in the Plato area based on their Earth-based visual, infrared, and radar signatures;

(b) Model radar scattering in the lunar regolith with an existing optical scattering computer program, and

(c) Demonstrate that the Moon can be mapped with 1-2km resolution with the 70cm Arecibo Radar.

Each of these items are discussed in seperate sections of this report. References, tables, and figures for all sections of this report appear at the end of this report.

I. PLATO AREA STUDY

The purpose of the Plato Area Study was to characterize lunar surface material in the Plato area based on their earth-based visual, infrared, and radar signatures. A Plato Study Consortium was formed to study the infrared, radar, and geologic features of the Plato area. Members of this consortium include:

D.L. Matson - Jet Propulsion Laboratory
H.J. Moore - USGS Menlo Park
R.S. Saunders - Jet Propulsion Laboratory
G.G. Schaber - USGS Flagstaff
R.W. Shorthill - Univ. of Utah Research Institute
T.W. Thompson - Planetary Science Institute
S.H. Zisk - NEROC Observatory

The first meetings of this Plato Consortium was held during November 1978. The first meeting in Flagstaff on 15-16 Nov. 1978 was attended by G. G. Schaber, R. W. Shorthill, and T. W. Thompson; the second meeting in Pasadena on 21 Nov. 1978 was attended by D. L. Matson, R. S. Saunders, and T. W. Thompson. The purpose of these first meetings were (1) to review the data collected to date (including new radar, IR, and visual data displays provided by Eric Eliason of USGS, Flagstaff and (2) to pursue first order questions about the Plato/Montes Jura area.

A third meeting of this Plato Consortium was held on 15-16 May 1979; meeting attendees included D. L. Matson, H. J. Moore, R. S. Saunders, R. W. Shorthill, and T. W. Thompson. The purpose of this meeting was to characterize various surface units, which could be defined by their optical and radar signatures.

Considerable attention was paid to the craters Plato M and Plato J and their environs since these craters appear to have unique spectral signatures. In addition the unique optical spectral signature of Plato M and Plato J, the terra units in the Plato area have a number of interesting features. The Montes Jura, the terra between Sinus Iridum, northern Mare Imbrium, and Mare Frigoris, have low radar reflectivites. Also craters Plato and Aristillus are surrounded by large haloes of low radar reflectivites.

The unusual nature of surface units region is illustrated in Figures 1-1, 1-2, and 1-3. Figures 1-1 and 1-2 show that the terra in the study region have high full moon albedo and low infrared eclipse temperatures as terra elsewhere on the moon. The 70cm radar map in Figure 1.2 shows that these terra have low radar reflectivities compared to nearby mare, while elsewhere on the moon the terra have higher reflectivity than nearby mare. The low reflectivity of the terra in the region is also observed at 7.5m wavelength as shown in Figure 1.3.

Figures 1.4 and 1.5 show high resolution 3.8cm radar maps of this area. Note that crater Plato is surrounded with a halo of low 3.8cm radar echoes as shown in Figure 1.4. Also, the Montes Jura and Montes Alpes have lower radar reflectivity than the nearby portions of Mare Imbrium as shown in Figure 1.5.

These unusual remote sensing signatures are related in part to the geologic history of this area. Like the rest of the Moon, the geology of the Plato, Montes Jura region is dominated by the formation of basins, subsequently filled by mare materials, and the formation of craters throughout the discernible geologic record.

The Imbrium basin is a multiringed basin with apparently three rings centered on 19°W, 38°N. Diameters of the rings are 670, 970, and 1340km (Hartmann and Wood, 1971). Landform morphologies produced by materials ejected from the Imbrium basin as well as other basin related materials dominate the surface topography of Montes Alpes within the region and Montes Apenninus to the south of the region (Wilhelms and McCauley, 1971). Many of the surfaces in the terra north of Mare Frigoris have morphologies that show Imbrium ejecta reached these terra areas and beyond. Imbrium basin related materials are also present as islands protruding through mare materials and these islands delineate the innermost ring.

Subsequent to the formation of the Imbrium basin, the crater of Sinus Iridum was excavated, chiefly between the first and second rings of the Imbrium basin. The Iridum crater, some 480km across, is only partly preserved -- the southeast rim is missing. To the west and north of Iridum in Montes Jura, thick deposits of ejecta from Iridum are super-posed on Imbrium related materials and Iridum must have excavated some Imbrium basin ejecta as well as pre-existing highlands materials. The ejecta are thickest near the Iridum rim and radially away from the rim the ejecta thins and secondary impact craters become dominant along the western-most, northern-most, and northeastern-most edges of Montes Jura.

After Iridum formed, the crater Plato was excavated by an impact event. Evidence for this is found near $52^{o}N$, $17^{o}W$, where secondary impact craters from Plato are super-posed on those of Iridum. Like Iridum, ejecta from Plato thickly mantles Imbrium related materials in the vicinity of the second Imbrium basin ring and Plato excavated Imbrium basin ejecta and perhaps pre-existing highlands. Secondary impact craters of Plato are present to the north, east, and west of Plato, but to the south they are covered by mare materials.

Extensive flooding by mare basalts filled the Imbrium basin and covered much of its ejecta and mountainous rings. The entire southeast of Iridum and its floor were also inundated by the volcanic floods of basalt. The floor of Plato was also

filled with basalts and isolated patches of its ejecta blanket are covered by mare basalts. Several sinuous rimae are also found on the flanks of Plato.

The volcanism occurred over a long period of time. Part of the problem that we are addressing is related to this fact. Some authors have suggested that KREEPY basalts may hve pre-dated and post-dated the formation of the Imbrium basin. Evidence for and against this postulate will be sought.

Photogeologic techniques reveal that there are several ages of mare basalt flooding. The oldest of these (≈3.75 b.y.) occurs south of Plato as an isolated patch within rather extensive mare basalts (≈3.6 b.y.) which also occur north of Aristillus and in Iridum. Most of the mare basalts in the area are about 3.2 b.y. old and they are found in Iridum, Mare Frigoris, Sinus Roris, Oceanus Procellarum, and in much of Mare Imbrium. Young mare basalts (3.0 b.y.) occur in northwest Mare Imbrium. The youngest mare basalts occur as flows in Mare Imbrium and on the boundary between Sinus Roris and Mare Frigoris (≈2.6 b.y.).

Throughout the history of the region impact craters formed and those observed range in age from the time of formation of the Imbrium basin to the recent past. Of particular interest here are the more recent ones, such as Aristillus (≈1.0 b.y.) and smaller fresh craters.

In summary, the major events in this area and their time sequence is as follows:

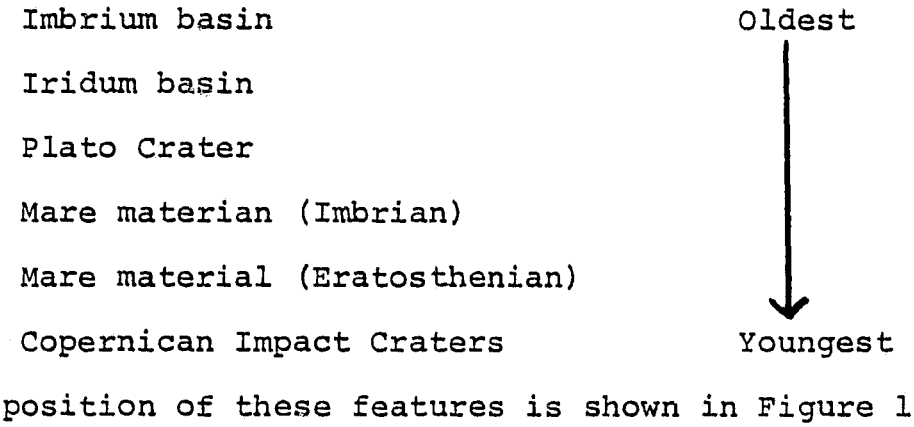

The position of these features is shown in Figure 1-6.

With this geologic history in mind, it is useful now to review the optical properties of various units in this area. This is given in Tables I-1, I-2, and I-3, where Table I-1 give spectral data related to craters, Table I-2 gives spectral data related to terra features and Table I-3 gives spectral features related to mare features. This spectral data was originally obtained by the SIPS (Spectral Imaging Photometer System), which is operated by Jet Propulsion Laboratory personnel and described by Johnson, Mosher, and Matson (1977). Dr. Joel Mosher of the Jet Propulsion Laboratory provided several computer printouts of this data.

As mentioned above an unusual feature of this area is crater Plato M which is surrounded by a holo of material with unusual optical properties as illustrated in Figure 1.7. Note that Plato M and its environs are the dark area just west of crater Plato. Plato M (53.0°N, 15.4°W) has a diameter of 8.4km, approximately eight percent of the diameter of crater Plato (51.4°N, 9.2°W).

Table I-1 summarizes the optical spectral characteristics of crater Plato J, Laplace D, and Plato M. These are terra craters in the vicinity of Sinus Iridium and crater Plato they display optical signatures similar to Plato J. All of these craters have steep spectral signatures with relatively high UV reflectivities and relatively low IR reflectivities. Table I-1 also shows optical data for other terra craters in the Plato Study. The floor, rim, halo of crater Aristillus have relatively high UV reflectivities and relatively low 1.0 μ reflectivities but these spectral signatures are not as steep as the signatures for Plato J. Crater Aristarchus, a young rayed crater in Western Mare Imbrium, has a steep spectral signature similar to Plato J. Also, the Tenerife Mountains and Mt. Pico, the possible surface expressions of the inner rims of the Imbrium basin, have spectral signatures similar to Plato J.

Almost all features in Table I-1 have spectral signatures similar to Plato J. However, Plato J is unique in that it's signature is the steepest. Also, the area surrounding crater Plato J appears to have spectral signatures similar to Plato J. One possible explanation is that Plato J's ejecta has covered the nearby areas. However, Plato J appears to be an older crater and the areas with this unique optical signature do not appear to be evenly distributed around Plao J. A more likely explanation is that the unique optical signatures associated with Plato J are derived from a subsurface deposit underneath a terra surface unit. In the vicinity of crater

Plato J, this overburden is relatively thin and smaller (kilometer sized) cratering events can excavate much of the subsurface deposit. In the vicinity of Laplace D and Plato M, the terra overburden is thicker. Here, only medium sized craters with sizes of a few tens of kilometers are deep enough to excavate and expose this subsurface deposit. Elsewhere on the moon, this deposit is non existant or too deep to be excavated by surface cratering events.

The rim of crater Plato has a spectral signature quite different from Plato J. Plato's rim has a high IR reflectivity whereas Plato J and the other terra craters given in Table I-1 have low IR reflectivity. All features listed in Table I-1 have relatively high UV reflectivity. Surprizingly, the different optical signatures for Plato J and Plato's rim may come from the same source. Malin (1974) has proposed that the "red" lunar features are expressions of premare KREEP emplacements. Also, Hawke and Head (1978) have mapped premare KREEP deposits in the southern portions of the Mare Imbrium basin floor. Hawke and Head (1978) find no photogeologic evidence for KREEP deposits in our study area. This would be expected if we are observing only surface manifestations on an underlying layer as described above. The unusual optical signatures associated with Plato J and similar features are possibly expressions of fresh KREEP exposures while the "red" rim of Plato is older KREEP exposures.

Table I-2 shows optical, infrared, and radar signatures of terra units in the Plato Study area. The unit entitled Iridium Flanks characterizes the terra west of Plato between Sinus Iridium and Mare Frigoris. This is the ejecta blanket associated with a large impact which occured after the Imbrium basin formation event and was subsequently flooded during the mare emplacement period. The unit entitled Plato's Halo describes the terra surrounding crater Plato and is the ejecta blanket for the crater Plato. The unit entitled Montes Jura is the terra east of crater Plato between northeastern Mare Imbrium and eastern Mare Frigori. This is the ejcta blanket emplaced during the Imbrium basin event. The unit entitled Aristarchus Plateau describes another lunar area which has low radar reflectivity (Zisk, et al., 1978).

All of the terra units given in Table I-2 have the low radar reflectivity. Elsewhere on the moon, terra units backscatter two to four times more power than adjacent mare units. Here, the terra units backscatter the same or less power than the nearby mare units. In addition, the infrared signatures for these terra units on the northern rim of Imbrium basin are not different from other terra. (Everywhere on the moon, the terra have lower eclipse temperatures than mare.) Thus, surface rocks, a source of radar backscatter, are more plentiful on the mare than on the terra. The lower radar backscatter of the terra units given in Table I-2 probably arises from higher electrical losses which attenuates echoes from subsurface scatterers. The mixing of a KREEP rich subsurface layer

into a terra overburden may cause this additional electrical loss. (On the Aristarchus Plateau, the source of the higher electrical loss is probably titanium rich pyroclastic deposits described by Zisk et al (1978).)

Table I-2 also shows differences in optical signatures in addition to the differences in the radar signatures. All of this suggests that the terra on the northern rim of the Imbrium basin has a different chemical composition than other terra units on the Moon.

Table I-3 shows the optical signatures for a number of mare units in the Plato Study area. The two units entitled Plato West and Plato East are mare units emplaced in the floor of crater Plato. These two units have optical signatures different from other nearby mare unts. It is possible that these differences are due to modification of lavas by host rocks in a subsurface layer which was KREEP rich.

In summary, the optical, radar, and infrared data for the terra on the northern rim of Imbrium basin are consistent with a model where a buried layer of KREEP is overlain by basin and crater ejecta. This buried KREEP layer is probably responsible for the following: (1) the unique optical signature of Plato J, (2) the splotches of Plato J - like optical signatures in the vicinity of Plato J, (3) the high UV, low IR optical signatures of the features in Table I-1, (4) the "red" rim of Plato, (5) the low radar reflectivity of the terra units, and (6) the differences in the optical signature of the Plato's floor and nearby mare units.

II. OPTICAL MODELING TASK

The purpose of this task was to model radar scattering in the lunar regolith with an existing computer program.

Prof. Martin Tomasko of the University of Arizona (a Consultant on this task) has modified his radiative transfer program for plane-parallel scattering layers to handle Rayleigh scattering by smaller rocks embedded in the lunar regolith. Both semi-infinite and finite models, illuminated by incident radar waves of arbitrary elliptical polarization, can now be treated. Strengths of both polarized and depolarized radar echoes, as a function of position on the lunar disk, have been computed for several idealized models of the regolith. Semi-infinite models, with single scattering albedos in the range 0.1 to 1.0, have been investigated. Finite models, with an underlying Lambert scattering surface, have also been studied for the situation of equal absorption and scattering lengths within the regolith. Calculations have been made for optical thicknesses in the range 0.25 to 1.0 and for Lambertian reflectivites of zero and unity.

An existing computer program for modeling of optical scattering from planetary atmospheres was adapted to the lunar radar case. In particular, scattering from the rocks imbedded in the regolith will occur because of the dielectric contrast with the surrounding powdery medium. Considering the long wavelengths involved, we can assume that each rock scatters

according to the Rayleigh phase matrix. Selection of the single scattering albedo depends on the dielectric contrast between rocks and powder. Absorption within the regolith powder, between successive scatterings, can be included in the single scattering albedo by using procedures developed by Hansen (1969a) and adopted by Pollack and Whitehill (1972). Optical thickness of the regolith was taken as either infinite or finite. In this context, optical thickness means the number of extinction lengths separating the lunar surface from the regolith base. Reflectivity of the Lambertian bedrock depends on the dielectric contrast at the interface. It will be taken to be arbitrary. Radiation reflected at the base will be considered to be unpolarized and uniform in the upward hemisphere, independent of the state of polarization and angular distribution of the incident radiation.

Our calculations were performed using a radiative transfer computer program developed for the analysis of Pioneer 10 and 11 photopolarimetry of Jupiter and Saturn (Tomasko et al., 1978). Based in part upon the van de Hulst doubling technique, as developed by Hansen (1969b; 1971), this program has exceptionally broad capability. Using plane-parallel geometry, the program computes the entire set of Stokes parameters (I, Q, U, V) for radiation scattered in an arbitrary direction, from an arbitrary planetary atmosphere, with an arbitrary scattering phase matrix, given an arbitrary set of Stokes parameters (I_o, Q_o, U_o, V_o), for radiation incident

from an arbitrary direction. Circularly and linearly polarized radiation are handled as special cases. Semi-infinite and finite (plus Lambert base) Rayleigh scattering models are the simplest cases. Inhomogeneity can be handled by successive layering if required. Only homogeneous semi-infinite and finite scattering models were considered. Refelction of radiation incident from below at the surface of the Moon was neglected.

Based in large part upon the electrical properties of lunar samples at microwave frequencies by Gold and his colleagues (Campbell and Ulrich, 1969; Gold, et al., 1976), the following assumptions are made. The dielectric constant for the dust between the buried scatterers is wavelength independent and has a value near 3.0, based upon measured solid-rock dielectric constants and their extrapolation to lunar soil densities (Carrier, et al., 1973). The electrical loss in the lunar subsurface is small and inversely proportion to wavelength. Thus, a radar absorption length will be 10 to 100 freespace wavelengths and independent of frequency. A Lambertian bedrock interface will be assumed to be parallel to the surface with depths of 1.75 to 70.0 meters for radar wavelengths of 70cm.

Within the model, these parameters are specified by the following quantities:

ε = Relative Dielectric Constant = 3.0 ± 1.0 (1)

$\tilde{\omega}$ = Single Scattering Albedo = 0.1 to 1.0 (2)

$= \varepsilon/(k+\eta)$

τ = Optical Depth of the Regolith = 0.25 to 1.0 (3)

$= (\kappa + \eta)$ Physical Depth

λ = Bedrock Reflectivity = 0.0 to 1.0 (4)

κ = Absorption Coefficient (cm^{-1}) (5)

η = Scattering Coefficient = N (6)

N = Number of Rocks per cm^3 (7)

σ = Scattering cross section of the Buried Rocks (8)

Observed radar cross-sections as a function of angle of incidence are given in Figure 2-1. Model computations for these values are given in Figures 2-2 through 2-8. Figures 2-2, 2-3, and 2-4 show computations for relative dielectric constants of 3.0 ± 1.0 and with optical depths of infinite (i.e. the scattering from a regolith bedrock interface is ignored) Figures 2-5 through 2-8 illustrate computations where ε, the dielectric constant is 3.0, optical depths, τ, are 0.25, 0.5, and 1.0 the single scattering albedo $\tilde{\omega}$ is 0.1, 0.5, and 1.0, and λ, the bedrock reflectivity is zero or unity.

For the semi-infinite models shown in Figures 2-2, 2-3, and 2-4, there is good agreement between model and observed polarized echo strengths. Both model and observations have a limb-darkening of $\cos^n(\theta)$ where $n \approx 3/2$. There is little

change in model computations for relatively large changes in dielectric constant from 2 to 4. Considering other planets such as Mars, Venus and Mercury, which polarized echoes proportional to $\cos^{3/2}(\theta)$, there is little new knowledge about the surface dielectric constants provided by this model.

The model predictions for depolarized diffuse scattering match the observations only for large angles of incidence. If angles of incidence are greater than 69° ($-\log \cos(\theta) > 0.45$) the model predicts limb darkening proportion to $\cos(\theta)$; the angular dependence that is observed. Also, our model predictions for the low absorption cases yields predictions similar to those neglecting multiple scattering (see Burns, 1969).

These semi-infinite models also predict an order-of-magnitude difference in backscattered power, when the single scattering albedo varies between 0.1 and 1.0. This may explain the mare-terra differences in average scattering (Thompson, 1978) and the intramare differnces observed in Mare Serenitatis, Mare Imbrium, and the Aristarchus Plateau (Thompson et al., 1973, Schaber et al., 1973, and Zisk et al., 1977). These differnces as suggested by Pollack and Whitehill (1972) arise from different absorptions from differing iron and titanium contents in the lunar soils.

In general, the models accounting for scattering from bedrock-regolith interface do not provide good matches with the observations as shown in Figures 2-5 through 2-8. Only a poorly reflecting bedrock underlying an optically thin regolith is a marginal possibility. This is expected for the terra, where the megaregolith, the debris layer overlying coherent basement rocks is a few kilometers deep (see Hartmann, 1973; Short and Forman, 1972; Thompson et al., 1979; Aggarawal and Oberbeck, 1979). This is unexpected for the mare, which are covered with regoliths of 3 to 10 meters thickness (Shoemaker and Morris, 1970). This suggests that the deeper portions of the regolith have few wavelength-sized dielectric discontinuities. Possibly, there are few dust pockets between rocks or there is a process which tend to stratify the rocks in to relatively smooth layers.

In summary this modelling effort has produced both positive and negative results. On the positive side, this model provides a good match with the observed polarized diffuse scattering which is proportional to $\cos^{1.5}(\theta)$. The model indicates that the $\cos^{1.5}(\theta)$ component is insensitive to choices of surface dielectric constant, so predictions of dielectric constant for other planetary surfaces must rely upon other means. This model also indicates that scatter albedo is important since it can modulate echo strengths by an order of magnitude, this provides a basis for interpretting mare-terra

and intramare scattering differences as responses to scattering losses from different surface chemical compositions, primarily iron and titanium content in the lunar case.

On the negative side, this model fails to predict depolarized diffuse scattering that is proportional to $\cos(\theta)$ for all angles of incidence. This may result from our original assumptions that surface rocks and large buried rocks were ignored. Future modelling efforts should use a Mie scattering approach to account for buried rocks of all sizes.

Also, modelling of a regolith-bedrock interface with a Lambertian scattering surface failed to predict observed scattering. This was expected for the terra, where regolith depths are on the order of a few kilometers. This was unexpected for the mare, where regolith depths are a few meters. This may result from several factors including stratification of ejecta blankets or the lack of dielectric contrast in the deeper portions of the regolith.

III. HIGH RESOLUTION RADAR OBSERVATIONS

The purpose of this task was to demonstrate that the moon can be mapped with 1-2km resolution with the 70cm Arecibo radar.

Radar observations of the moon were conducted using the 430 MHz (70cm wavelength) radar at the Arecibo Observatory during December 1979. Pre-observation preparations included the generation of ephermerides using data provided by Drs. James Williams and Charles Yoder of the Jet Propulsion Laboratory. The basic data provided by Drs. Williams and Yoder was modified to give radar processing parameters for the observations.

Radar data was collected in two nights. The Mare Serenitatis area was observed on 16 Dec. 1978; the Plato-Montes Jura area was observed on 18 Dec. 1978. The radar geometry and processing parameters for these observations are given in Tables 3-1, 3-2, and 3-3 and Figures 3-1 and 3-2. (Tables 3-1 and 3-2 give details for the radar geometry depicted in Figures 3-1 and 3-2).

Table 3-3 gives various processing prarmeters for these new observations as well as those used in 1966 to 1969. The new data will give a considerable improvement in resolution. Range resolution was improved by a factor of 1 to 4; frequency reoslution is 2 times better for the Mare Serenitatis area and 4 times better for the Plato area.

The data acquired in December was analyzed between January 1979 and May 1979. The first steps in the data analysis were (1) to establish the basic integrity of the data and (2) to rearrange the data so that Delay-Doppler spectra could be obtained with a minimum of computer operations. These first steps met with difficulties that made further processing of the data impractical.

A necessary first step in the post-run data reduction was to make crude Doppler spectra of the data in order to demonstrate that the radar were coherent. Thus, crude spectra were obtained for every 50th range sample, where each spectra consisted of 32 points yielding a frequency resolution of 0.33 hz . For comparison, the desired mapping resolution was 1024 points yielding a spectral resolution of 0.12 hz These crude spectra showed an expected echo drift of (1.14 hz/ minute). This expected echo drift would in turn complicate further data analysis since an early stage of data analysis would have to artifically "unwind" echoes by this drift.

Another early data processing step rearranged echoes in order to facilitate the FFT processing. In particular, the radar data was acquired such that the (consecutive) range samples are combined into one data record and written on magnetic tape. Then, echoes from consecutive pulses were written as consecutive records on the magnetic tape. The ensuing FFT processing of these echoes needed to strip consecutive

echoes from the same range sample and form a new data record. This "corner-turning" matrix inversion was implemented, but turned out to be a very expensive computer operation. An unexpensive alternative to use existing software at the Arecibo Observatory did not materialize.

These two difficulties, the expected echo drifting and the expensive matrix inversions, meant that processing of the December 1979 observations far exceeded the budget allotted for this task. Thus, work on this task was stoped before Delay-Doppler maps could be produced. Although, the post run analysis was a failure, it should be pointed out that this task did demonstrate that the data for high resolution mapping could be acquired using the 430MHz (70cm wavelength) radar at the Arecibo Observatory. Pre-run preparations, the generation of ephemerides and planning aids (such as those shown in Figures 3-1 and 3-2 and Tables 3-1 and 3-2) and the integration of the JPL generated ephemerides into Arecibo Data Acquisition programs were successful. Also, computer programs now exist for immediate postrun analysis to assure data quality.

ACKNOWLEDGEMENT

Dr. Henry J. Moore of the United States Geologic Survey, Menlo Park, California contributed to the geologic summary of the Plato Area given in Part I of this report. Dr. Joel Mosher contributed to Plato Study by providing several print-outs of SIPS optical data. Mr. Clifford Stoll of the University of Arizona performed many of the computer computations for the Optical Modelling Task described in Part II of this report. Dr. Donald B. Campbell and Mr. Reyes of the Arecibo Observatory staff provided invaluable help in conducting the radar observations described in Part III of this report.

REFERENCES

H.R. Aggarwal and V.R. Oberbeck (1979), Monte Carlo Simulation of Lunar Regolith and Implications, Tenth Lunar and Planetary Conference (Abstract) pp. 6-8.

A.A. Burns (1969), Diffuse Componenet of Lunar Radar Echoes, J.G.R., 74, pp. 6553-6566.

M.J. Campbell and J. Ulrichs (1969), Electrical Properties of Rocks and their Significance for Lunar Radar Observations, J.G.R., 74, pp. 5867-5881.

W.D. Carrier III, J.K. Mitchell, and A. Mahmood (1973), The Relative Denisty of Lunar Soil, Proc. of the Four Lunar Sci. Conf., v. 2, pp. 2403-2411.

T. Gold, E. Bilson, and R.L. Baron (1976), Electrical Properties of Apollo 17 Rock and Soil Sampler and a Summary of the Electrical Properties of Lunar Material at 450MHz Frequency, Proc. Lunar Science Conf. 7th, v. 3, pp. 2593-2603.

T. Hagfors (1967), A Study of the Depolarization of Lunar Radar Echoes, Radio Science, v. 2 (new series), pp. 445-465.

J.E. Hansen (1969a), Absorption Line Formation in a Scattering Planetary Atmosphere, Astrophy. J., v. 158, pp. 337-349.

J.E. Hansen (1969b), Radiative Transfer by Doubling Very Thin Layers, Astrophy. J. v. 155, pp. 565-573.

J.E. Hansen (1971), Multiple Scattering of Polarized Light in Planetary Atmospheres. I the Doubling Method, J. Atmos. Sci., v. 28, pp. 120-125.

W.K. Hartmann (1973), Ancient Lunar Megaregolith and Subsurface Structure, Icarus, v. 18, pp. 634-636.

W.K. Hartmann and C.A. Wood (1971), Moon: Origin and Evolution of Multi-ring Basins, The Moon, v. 3, pp. 3-78.

B.R. Hawke and J.W. Head (1978), Lunar KREEP Volcanism: Geologic Evidence for History and Mode of Emplacement, Proc. Lunar Planet. Sci. Conf. 9th, v. 3, pp. 3285-3309.

T.V. Johnson, J.A. Mosher, and D.C. Matson (1977), Lunar Spectra Types: A Northern Hemisphere Mosaic, Proc. Lunar Sci. Conf. 8th, v. 1, pp. 1013-1028.

M.C. Malin (1974), Lunar Red Spots: Possible Pre-Mare Materials, Earth and Planetary Science Letters, v. 121, pp. 331-341.

J.B. Pollack and L. Whitehill (1972), A Multiple Scattering Model of the Diffuse Component of Lunar Radar Echoes, J.G.R., v. 77, pp. 4289-4303.

G.G. Schaber, T.W. Thompson, and S.H. Zisk (1973), Lava Flows in Mare Imbrium: An Evaluation of Anomalously Low Earth-based Radar Reflectivity, The Moon, v. 13, pp. 395-423.

E.M. Shoemaker and E.C. Morris (1970), Physical Properties of the Lunar Regolith Determined from Surveyor Television Observations, Radio Science, v. 5, pp. 129-155.

N.M. Short and M.L. Forman (1972), Thickness of Impact Crater Ejecta on the Lunar Surface, Modern Geology, v. 3, pp. 69-91.

T.W. Thompson (1978), High Resolution Lunar Radar Map at 7.5 Meter Wavelength, Icarus, v. 36, pp. 174-188.

T.W. Thompson, K.A. Howard, R.W. Shorthill, G.C. Tyler, S.H. Zisk, E.A. Whitaker, G.G. Schaber, and H.J. Moore (1973), Remote Sensing of Mare Serenitatis, Chapter 33, Part A of Apollo 17 Preliminary Science Report, NASA Washington, D.C.

T.W. Thompson, W.J. Roberts, W.K. Hartmann, R.W. Shorthill, and S.H. Zisk (1979), Blocky Craters: Implications about the Lunar Megaregolith, accepted for publication in The Moon and Planets.

M.G. Tomasko, R.A. West, and N.D. Castillo (1978), Photometry and Polarimetry of Jupiter at Large Phase Angles, Icarus, v. 33, pp. 558-592.

D.E. Wilhelms and J.F. McCauley (1971), Geologic Map of the Near Side of the Moon: U.S. Geol. Survey Mis. Geol. Inv. Map I-703.

S.H. Zisk, C.A. Hodges, H.J. Moore, R.W. Shorthill, T.W. Thompson, E.A. Whitaker, and D.E. Wilhelms (1977), The Aristarchus - Harbinger Region of the Moon: Surface Geology and History from Recent Remote Sensing Observations, The Moon, v. 17, pp. 59-99.

FULL MOON PHOTOGRAPH

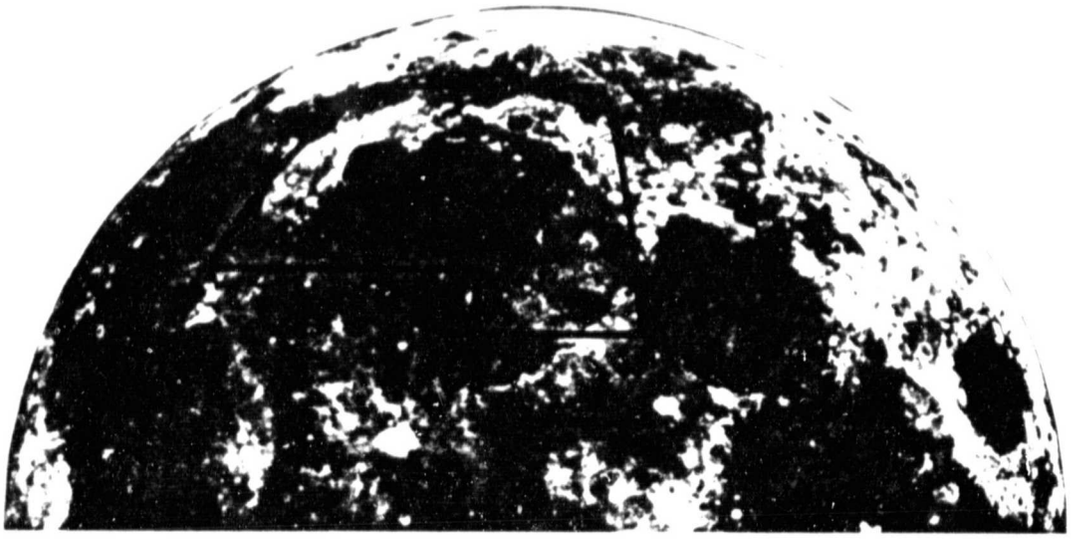

MOSAIC OF LOW SUN ANGLE PHOTOS

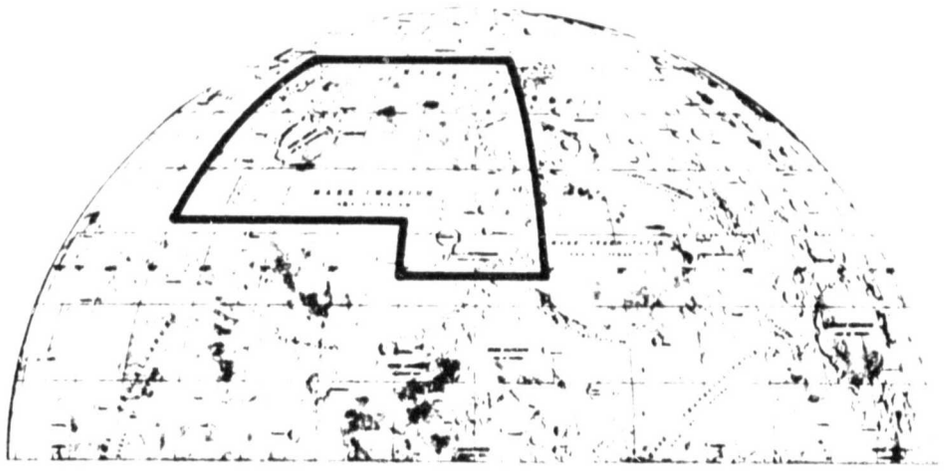

Figure 1-1 Optical Appearance of the Plato/Montes Jura Study Area. Note that terra in this region have the same appearance as terrae elsewhere on the Moon.

70 cm RADAR MAP

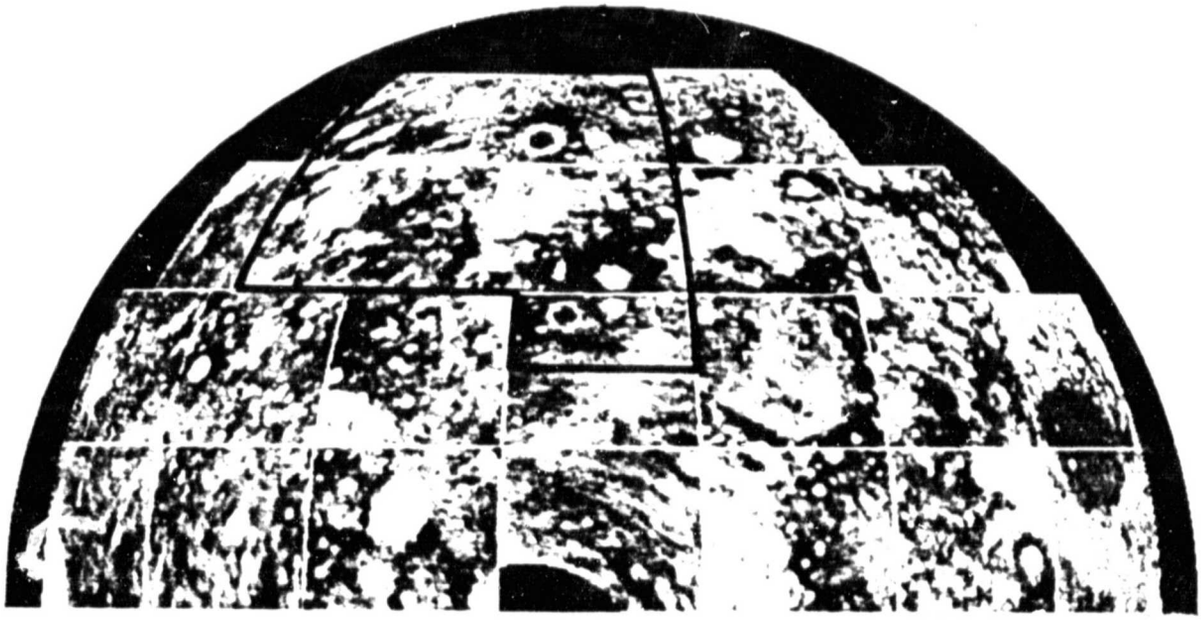

IR ECLIPSE TEMPERATURE MAP

Figure 1-2 70cm Radar and IR (10 micron) eclipse temperatures of the Plato/Montes Jura Study Area. Note the low radar reflectivity associated with terra in the study area and the dark haloes associated with crater Plato.

Figure 1-3 7.5m radar map of the Plato/Montes Jura Area. Note the extreme low radar reflectivity associated with the terra between Northern Mare Imbrium and Mare Frigoris.

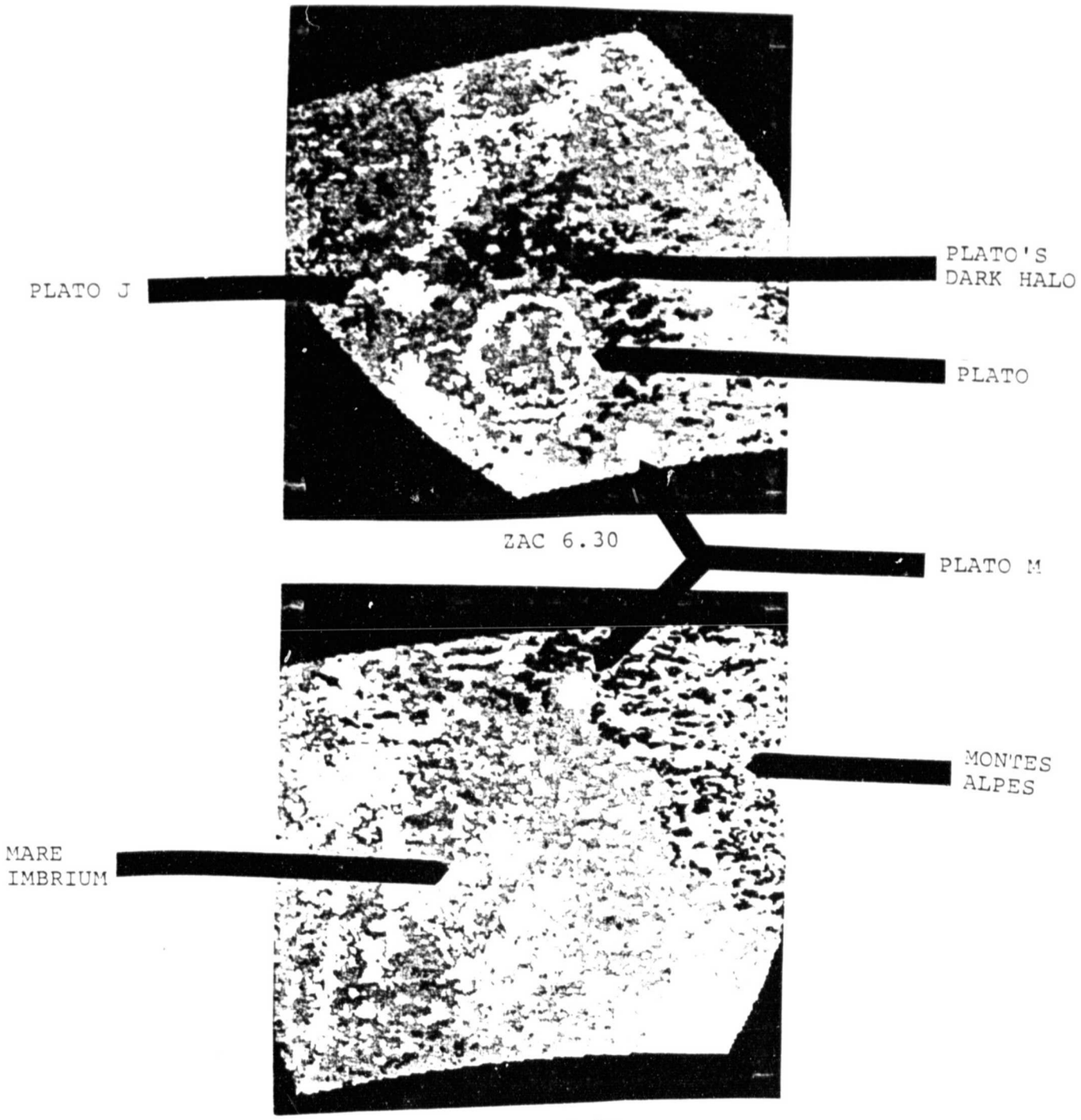

Figure 1-4 3.8cm Depolarized Radar Maps of Crater Plato (9.2°W, 51.4°N, 100.0km, ZAC 6.30) and Alpes-Mare Imbrium boundary (ZAC 5.30). Note the radar dark halo surrounding Plato and the low reflectivity of the Alpes area.

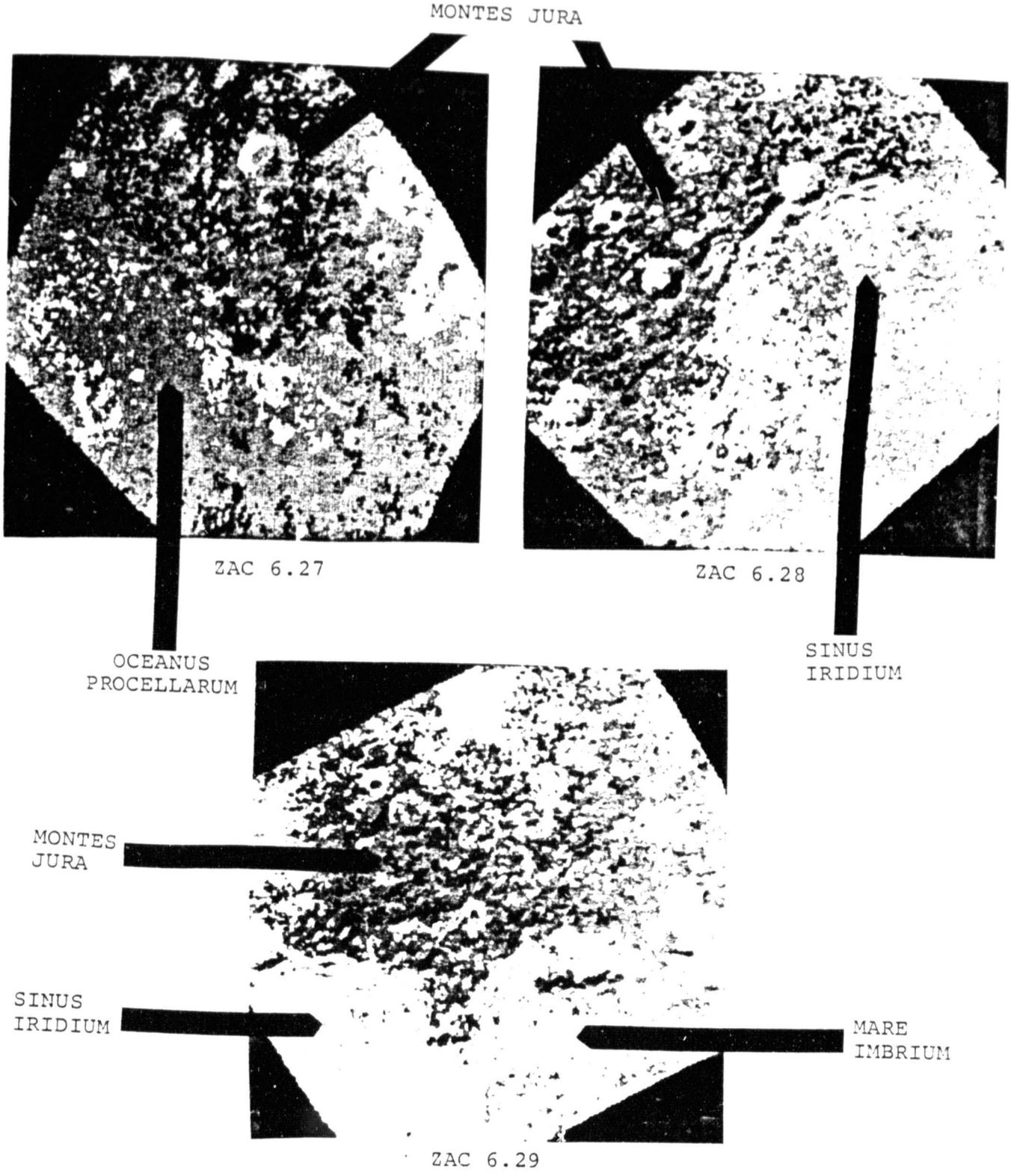

Figure 1-5 3.8cm Radar Maps of Sinus Iridium (31.2°W, 44.4°N, 260km diameter, ZAC 6.28 and ZAC 6.29). The large crater in the center of ZAC 6.27 is Mairan (43.4°W, 41.6°N, 41km diameter). Note that the terra, Montes Jura has a low radar reflectivity.

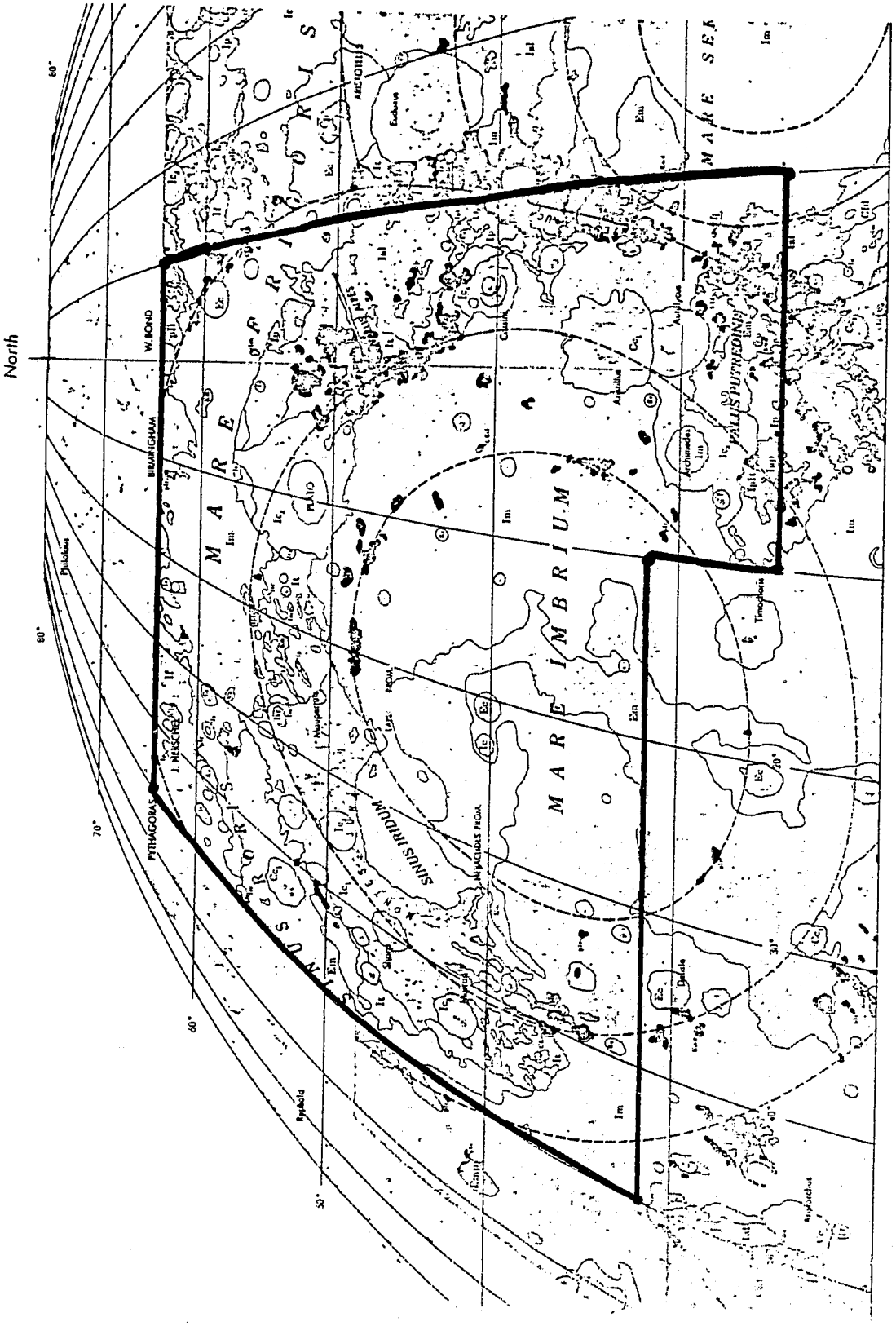

Figure 1-6 The Plato-Montes Jura Study Area. Background Geologic Map from Wilhelms and McCauley (1971).

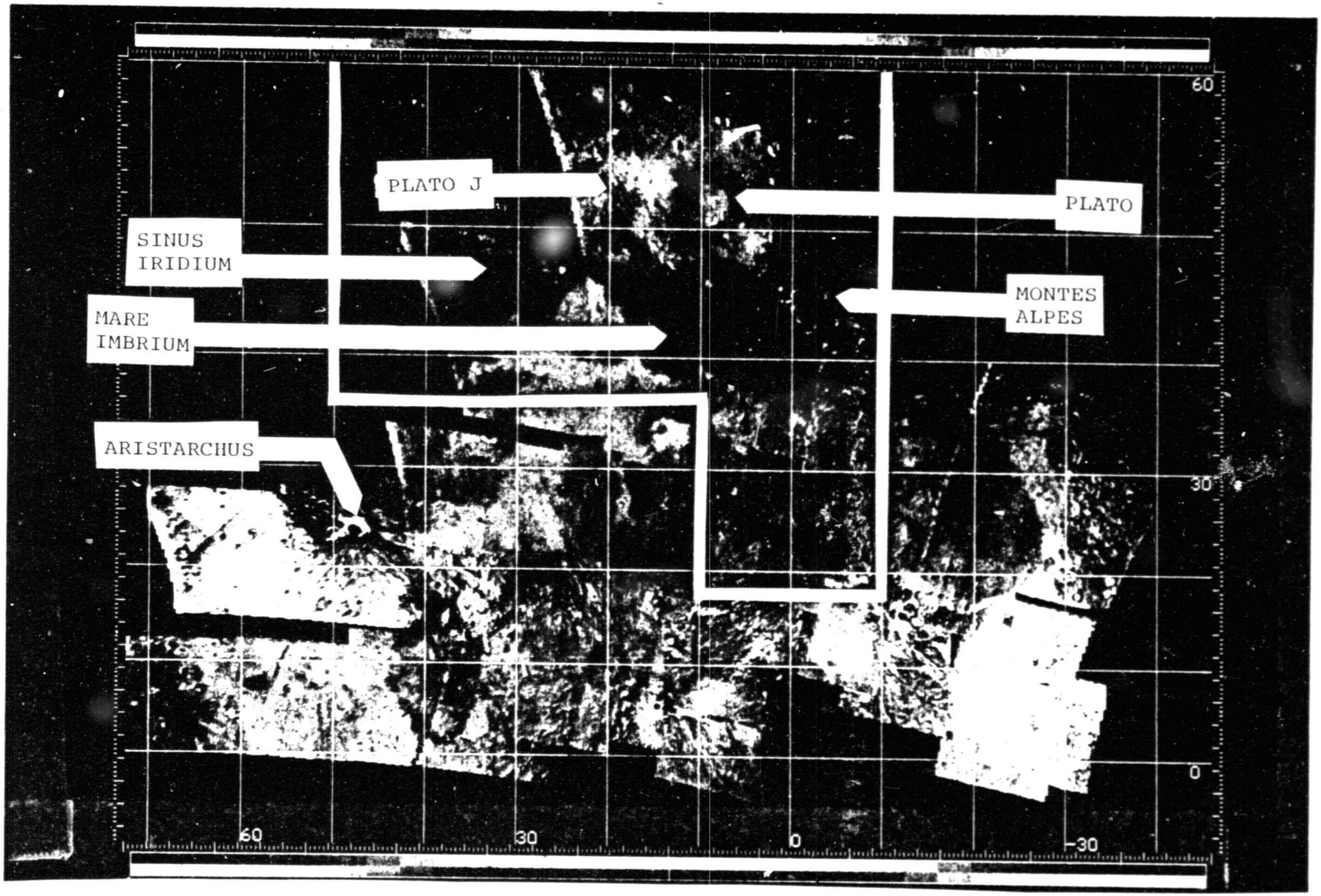

Figure 1-7 Spectral Imaging Photometer System (SIPS) Ratio (3800Å/5600Å) Data for Northern Hemisphere of the Moon. Craters Plato and Plato J are at the top of the photograph. Note the unusual signature for Plato J.

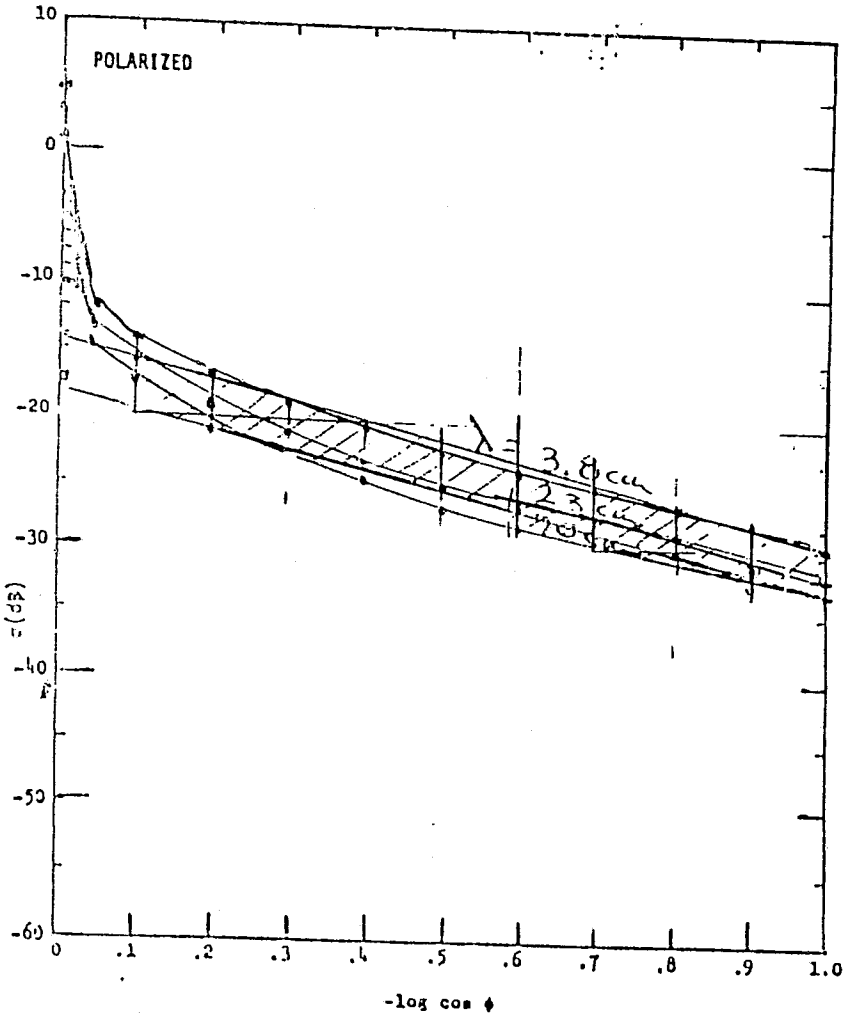

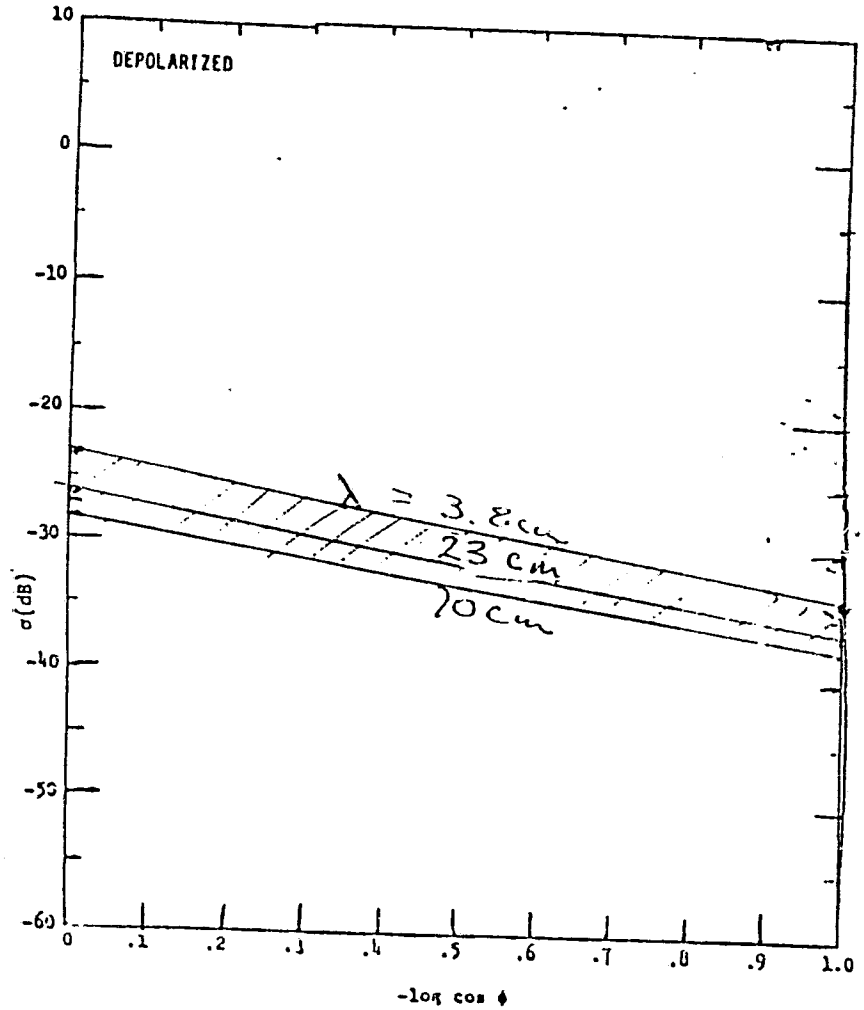

Figure 2.1 Observed Polarized and Depolarized Radar Cross-sections for the Moon. Data from Hagfors (1967). Note that the same cross hatched area is shown in Figures 2-2 through 2-10.

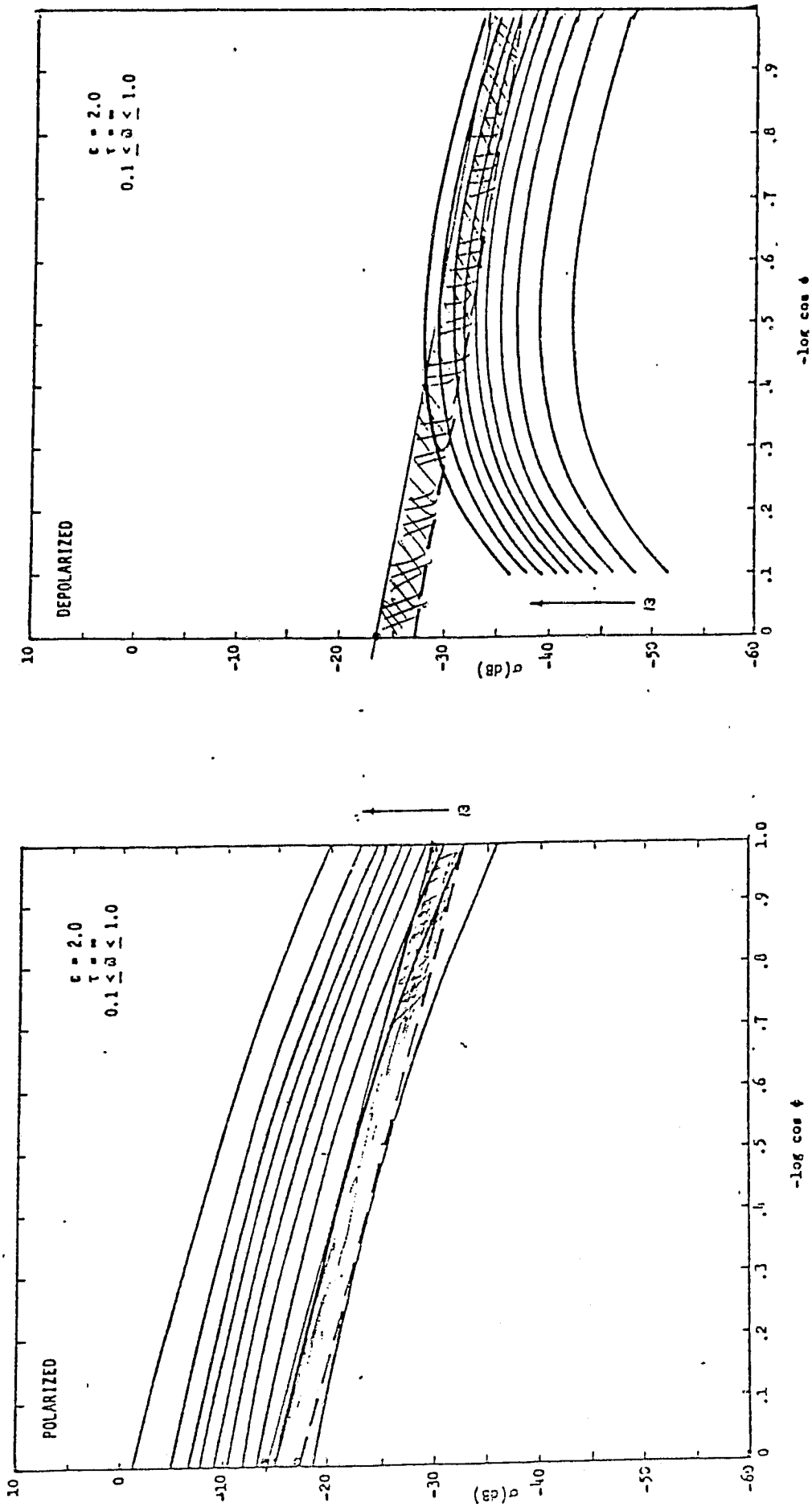

Figure 2.2 Computed Radar Backscatter for the Semi-infinite model with ε = relative dialectric constant = 2.0 $\tilde{\omega}$ = single scattering albedo = 0.1 to 1.0. Note the relatively good match of observed polarized backscatter with the model.

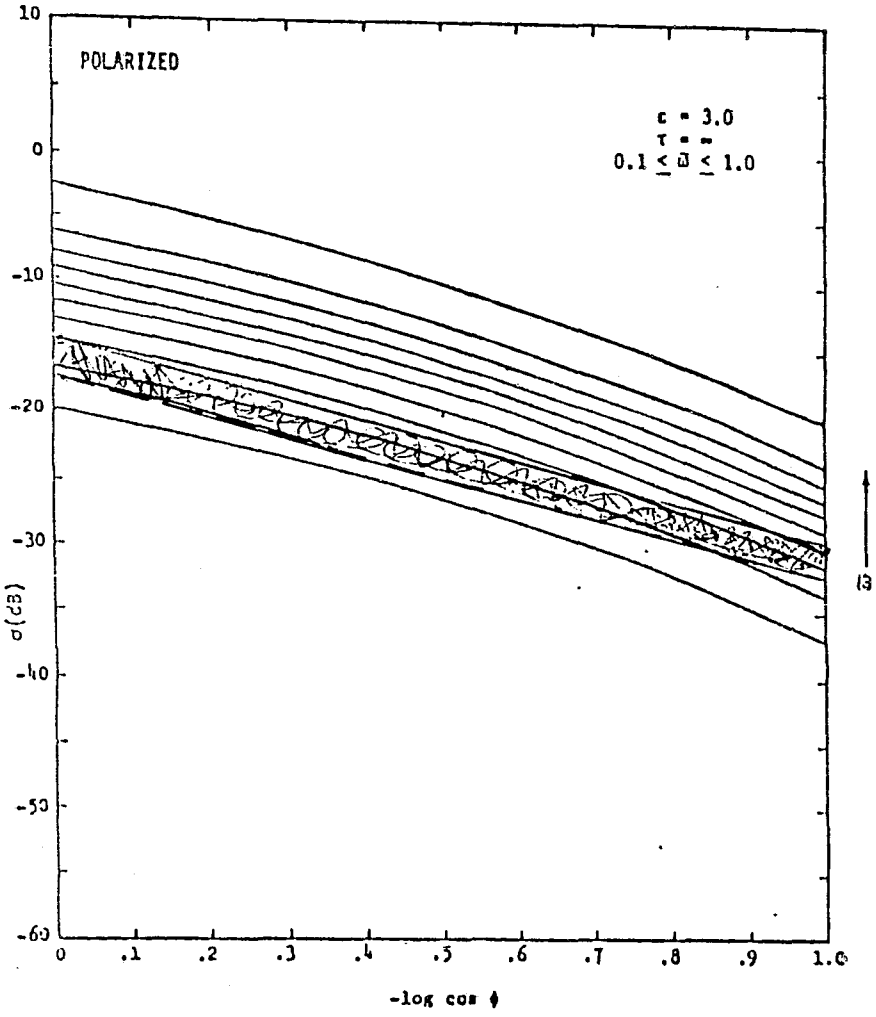

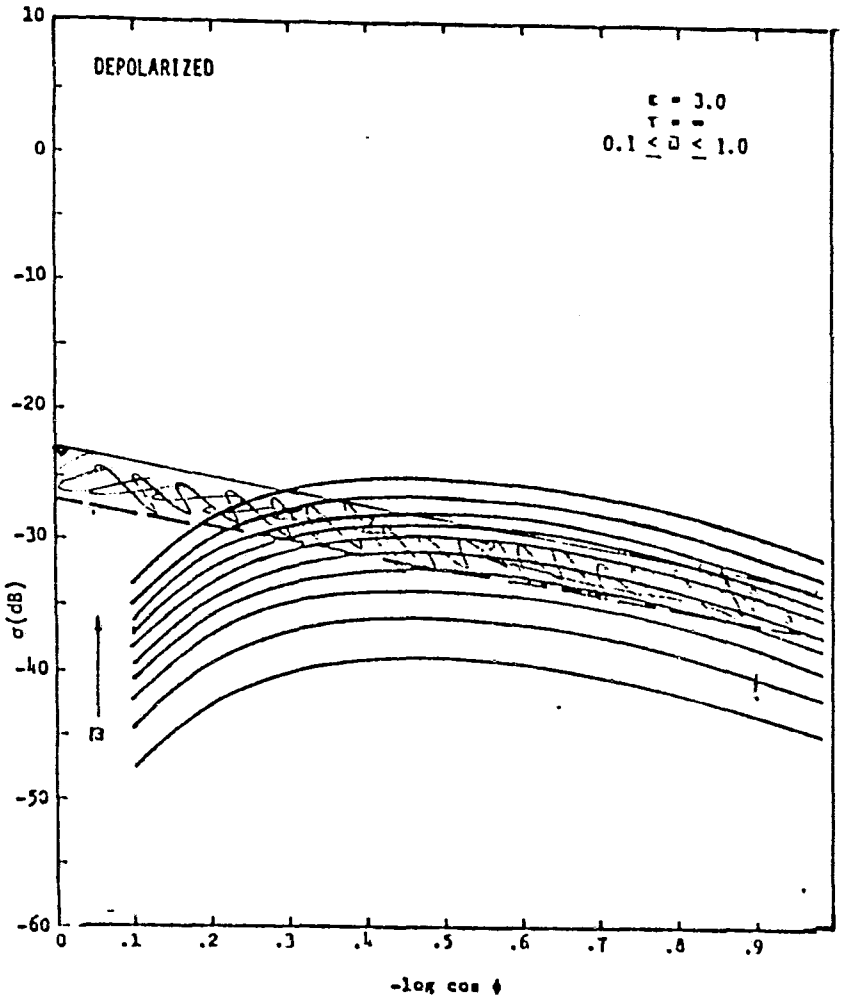

Figure 2.3 Computed Radar Backscatter for the Semi-infinite model with ε = relative dielectric constant = 30 $\tilde{\omega}$ = single scattering albedo = 0.1 to 1.0. Note the relatively good match of observed polarized backscatter with the model.

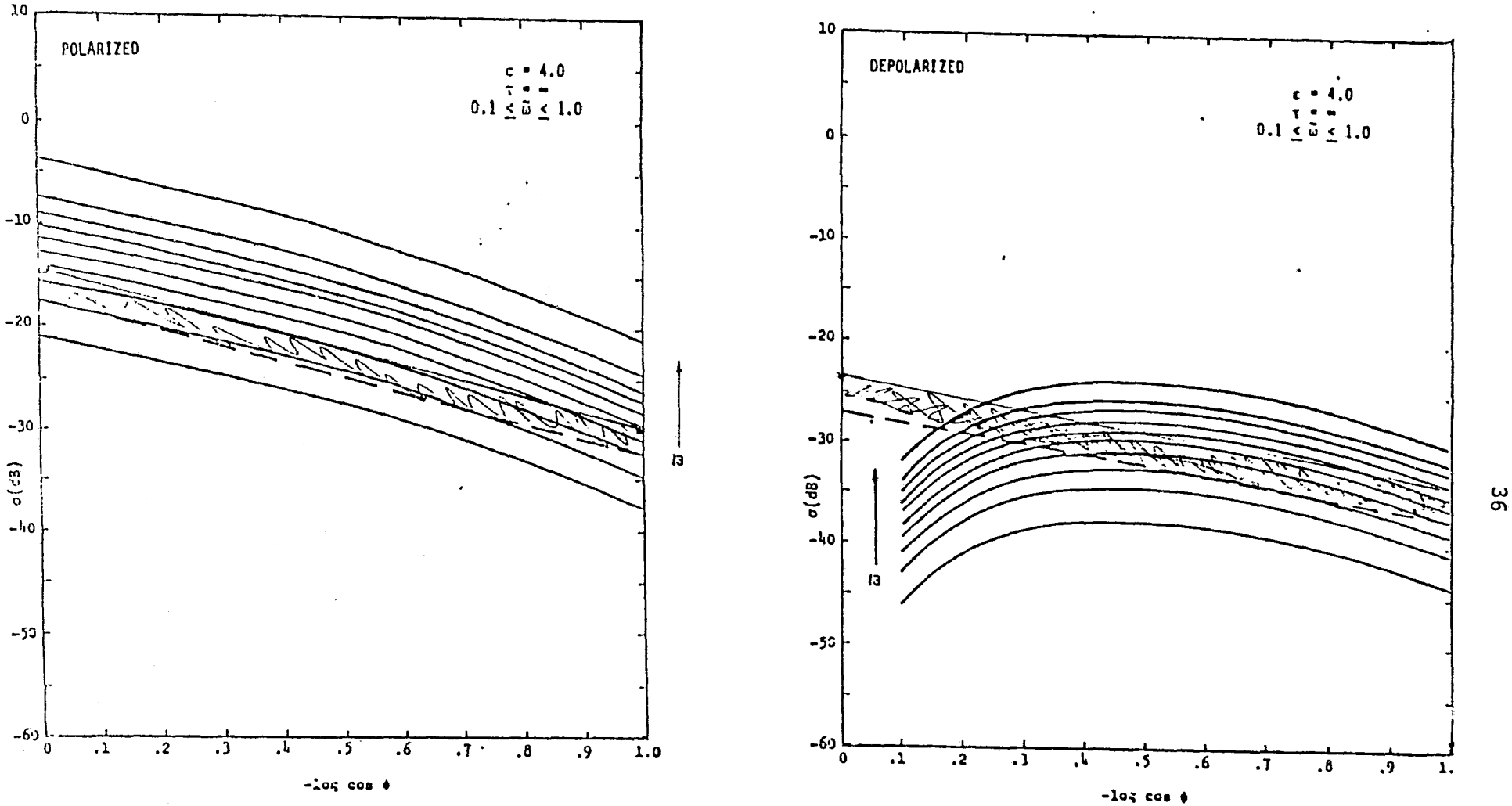

Figure 2.4 Computed Radar Backscatter for the Semi-infinite model with ε = relative dielectric constant = 4.0 $\tilde{\omega}$ = single scattering albedo = 0.1 to 1.0. Note the relatively good match of observed polarized backscatter with the model.

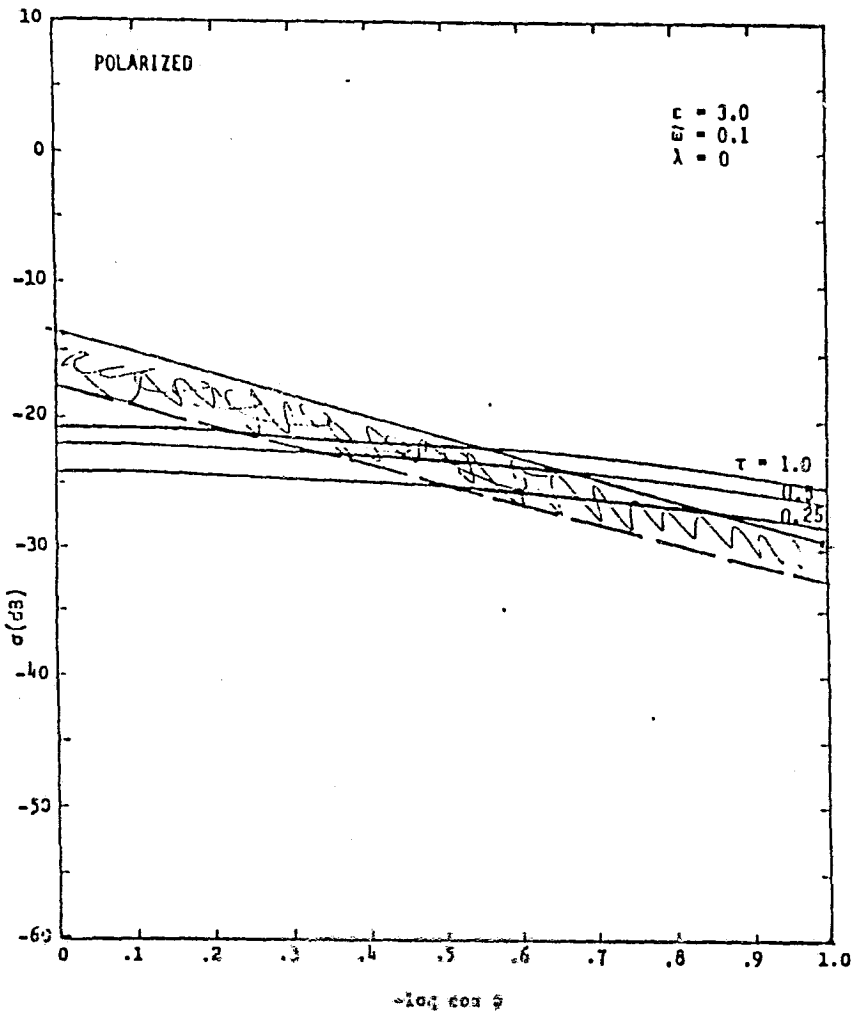

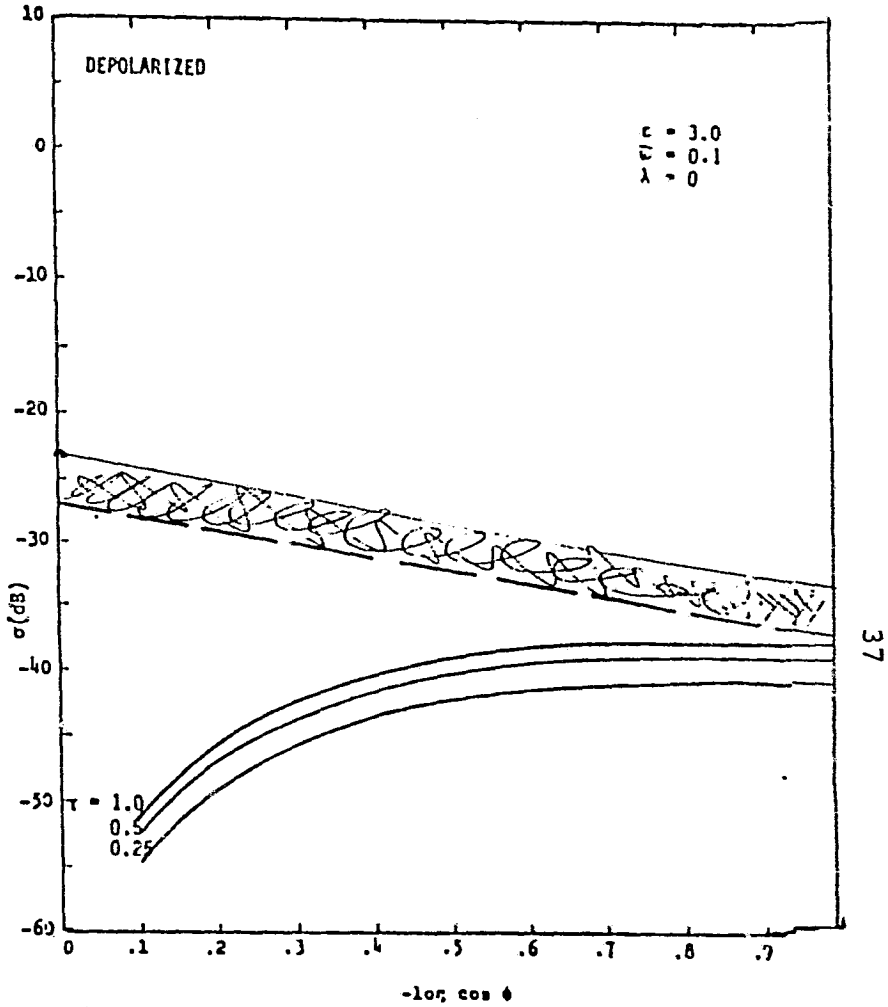

Figure 2.5 Computed Radar Backscatter for Finite Regolith and Lambertian Regolith - Bedrock Interface with:

ε = Relative Dielectric Constant = 3.0
$\tilde{\omega}$ = Single Scattering albedo = 0.1
τ = Optical Depth of the Regolith = 0.25 to 1.0
λ = Bedrock Reflectivity = 0.0

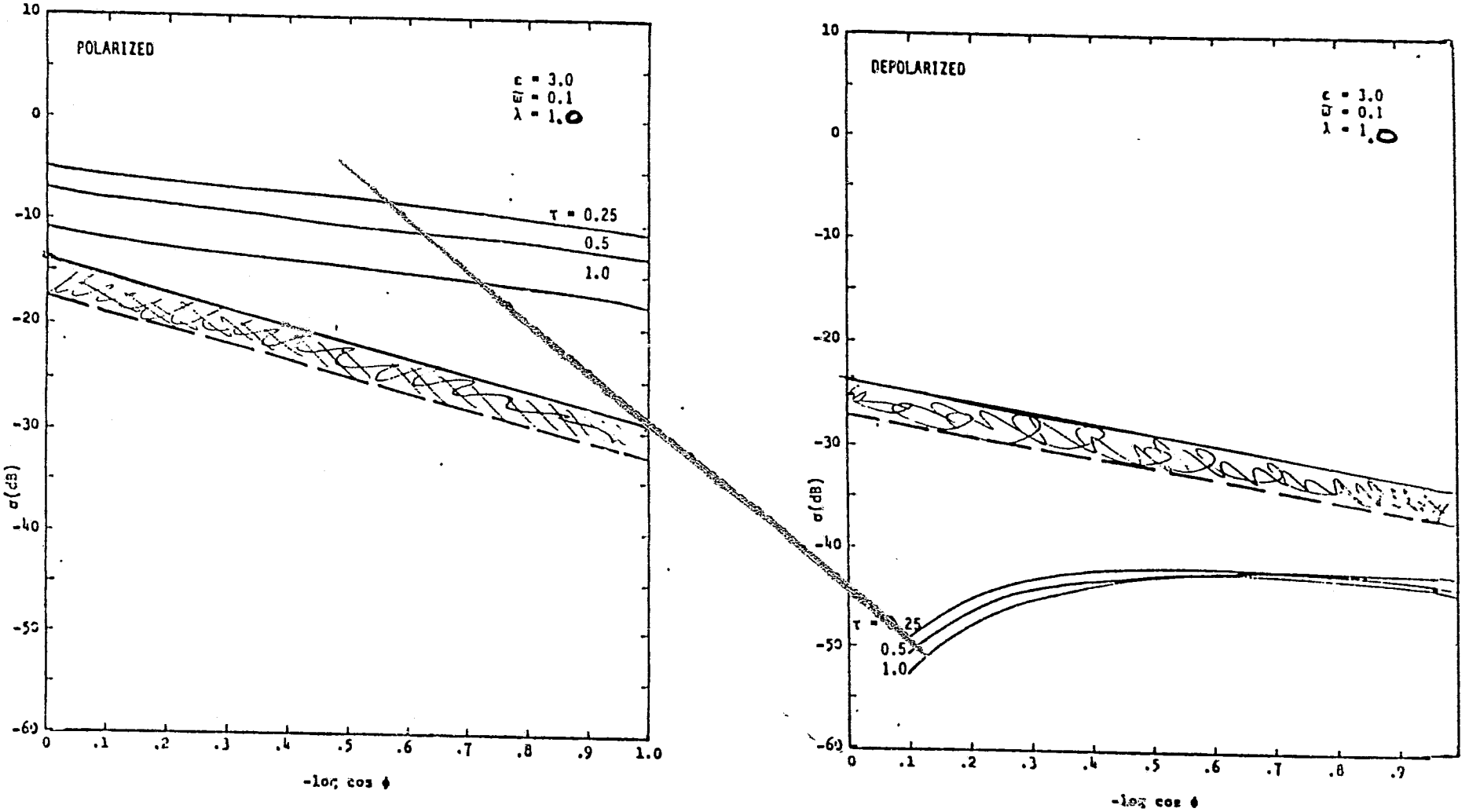

Figure 2.6 Computed Radar Backscatter for Finite Regolith and Lambertian Regolith - Bedrock Interface with:

ε = Relative Dielectric Constant = 3.0
$\tilde{\omega}$ = Single Scattering albedo = 0.1
τ = Optical Depth of the Regolith = 0.25 to 1.0
λ = Bedrock Reflectivity = 1.0

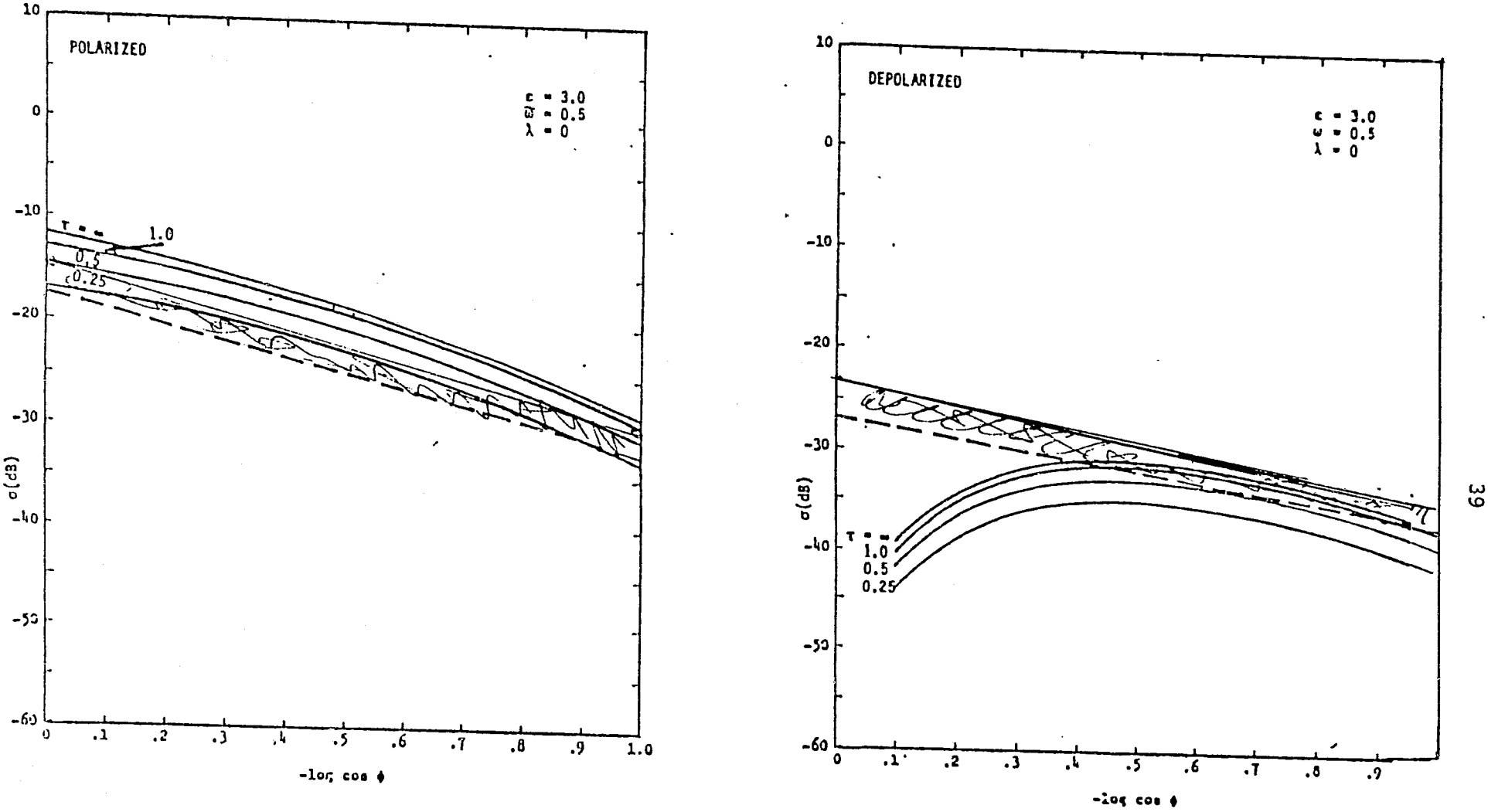

Figure 2.7 Computed Radar Backscatter for Finite Regolith and Lambertian Regolith - Bedrock Interface with:

ε = Relative Dielectric Constant = 3.0
$\tilde{\omega}$ = Single Scattering albedo = 0.5
τ = Optical Depth of the Regolith = 0.25 to 0
λ = Bedrock Reflectivity = 0.0

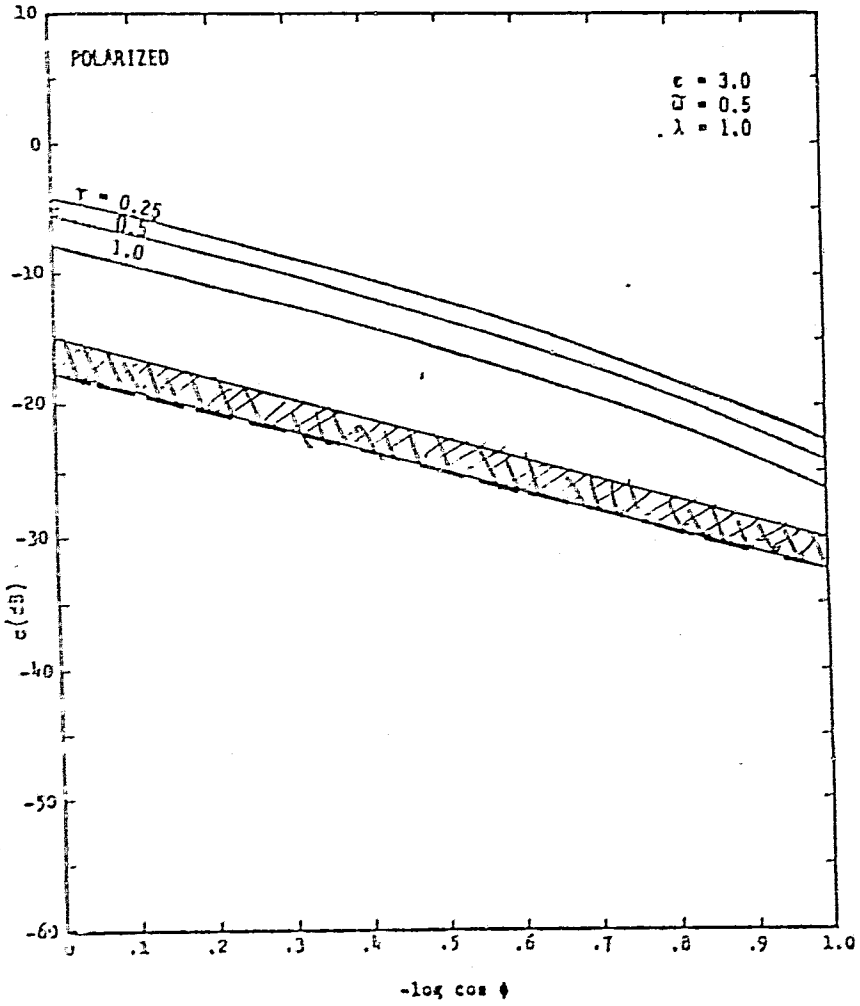

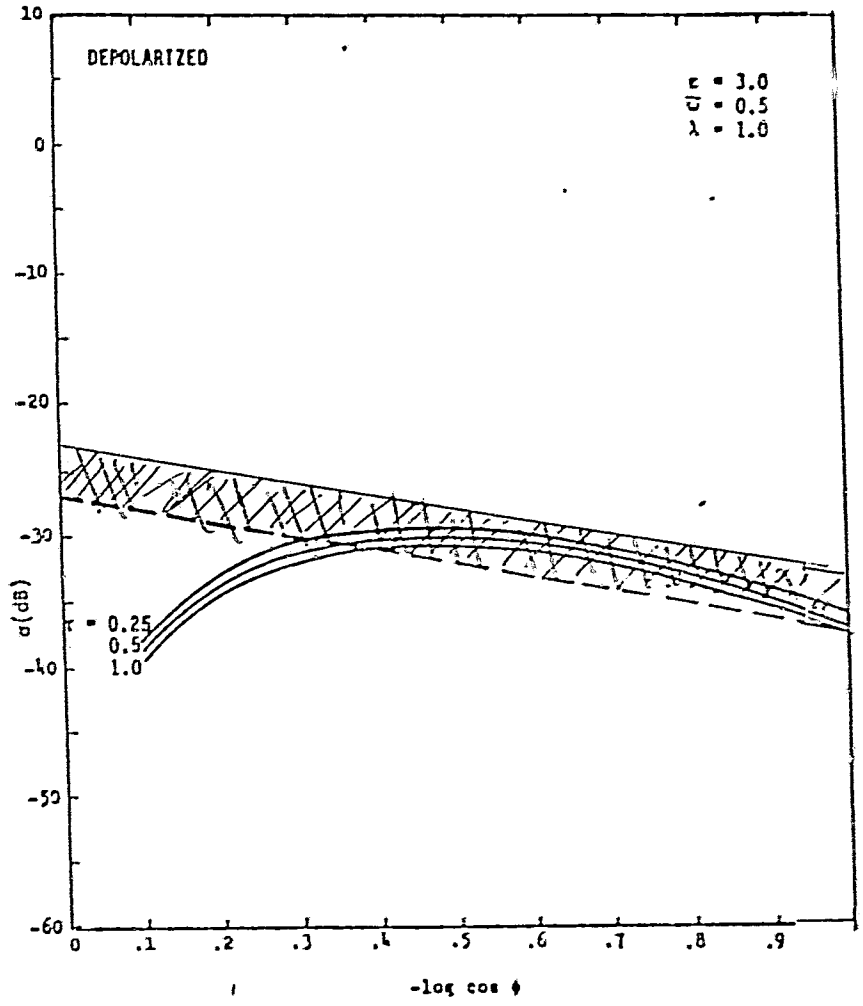

Figure 2.8 Computed Radar Backscatter for Finite Regolith and Lambertian Regolith - Bedrock Interface with:

ε = Relative Dielectric Constant = 3.0
$\tilde{\omega}$ = Single Scattering albedo = 0.5
τ = Optical Depth of the Regolith = 0.25 to 1.0
λ = Bedrock Reflectivity = 1.0

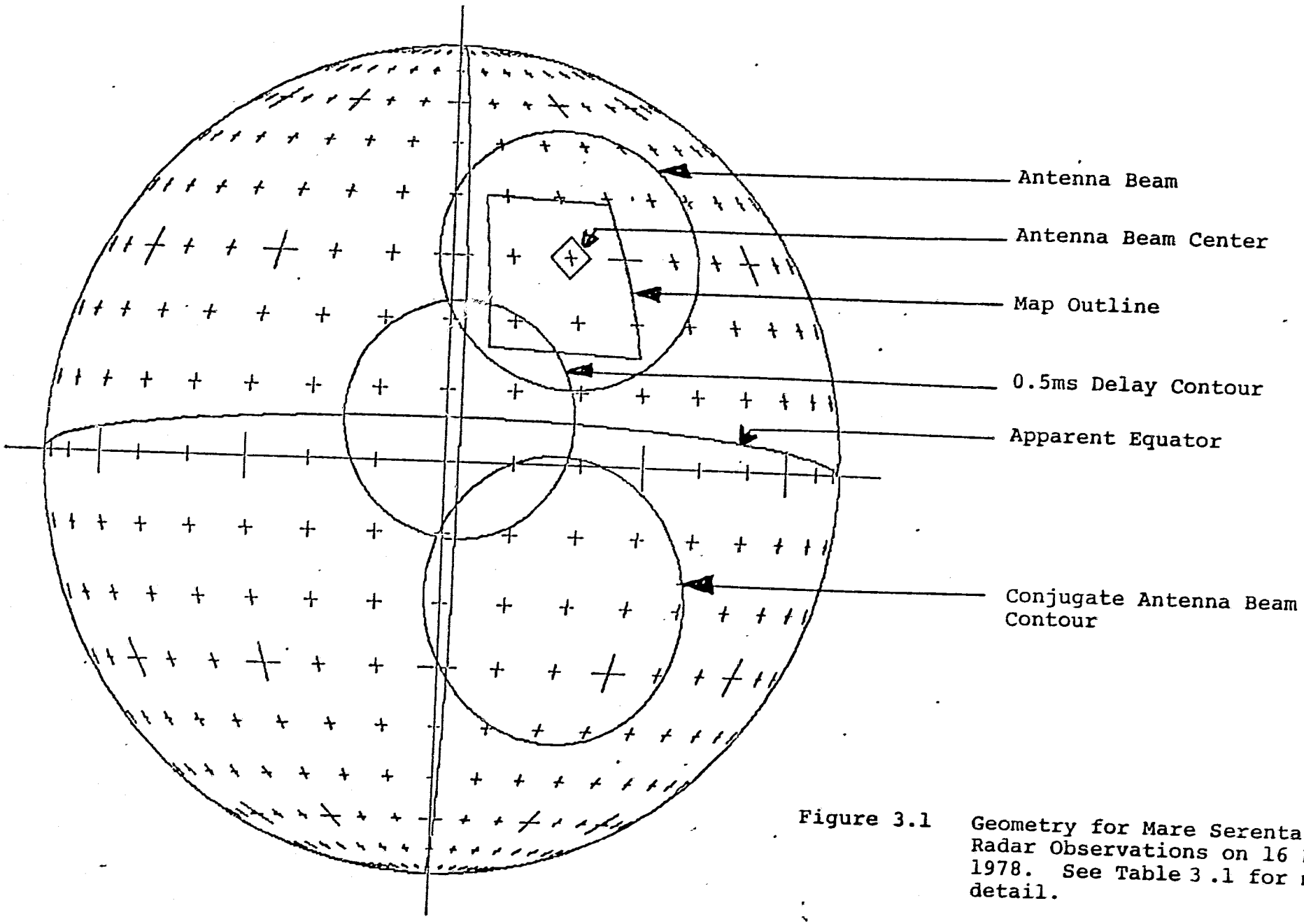

Figure 3.1 Geometry for Mare Serentatis Radar Observations on 16 Dec. 1978. See Table 3.1 for more detail.

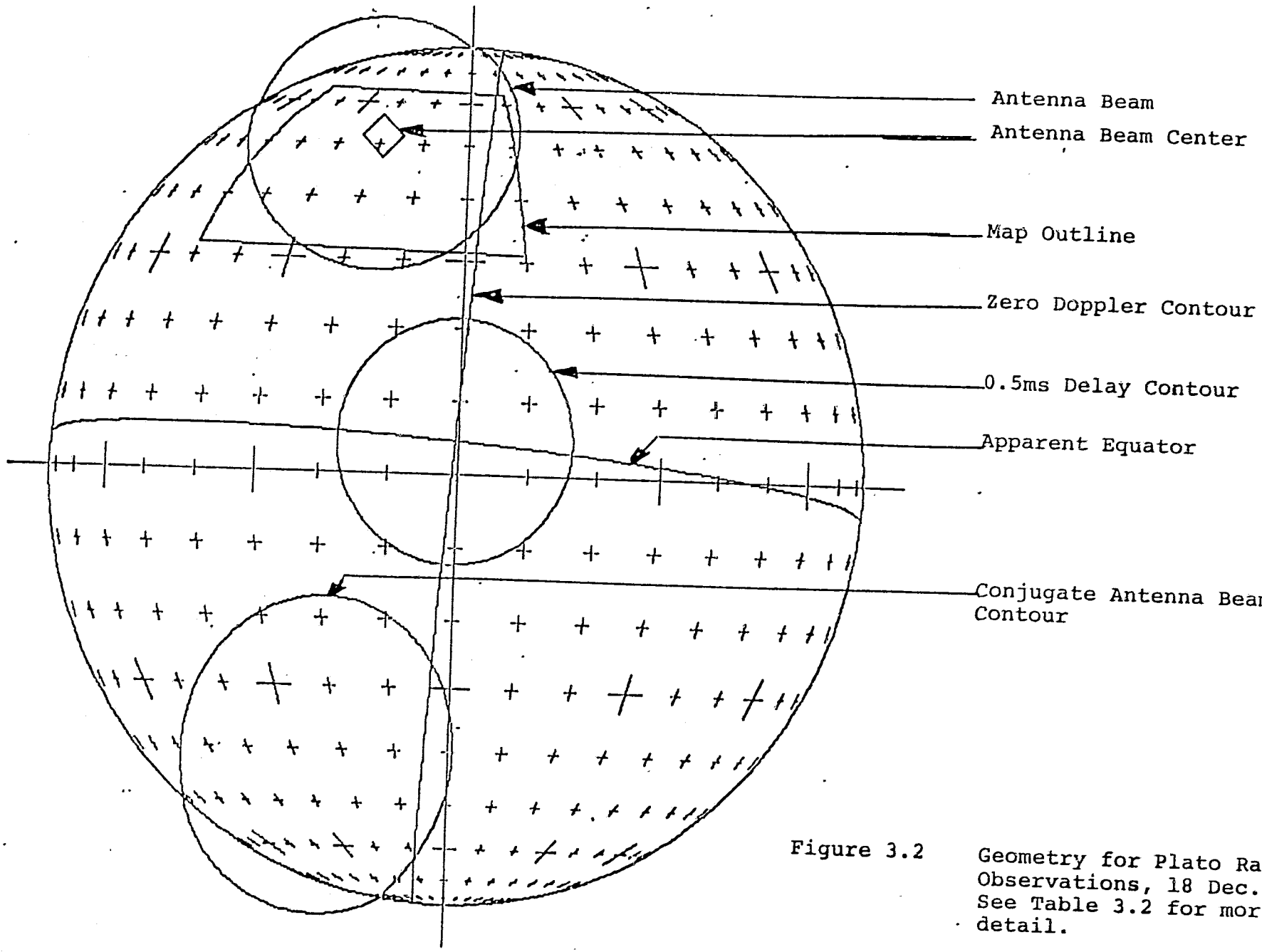

Figure 3.2 Geometry for Plato Radar Observations, 18 Dec. 1978. See Table 3.2 for more detail.

TABLE I-1

OPTICAL SPECTRAL SIGNATURES
FOR TERRA CRATERS
AND OTHER "TERRA" FEATURES
IN THE PLATO STUDY AREA

OBJECT	LON	LAT	3800A°	5600A°	8500A°	10500A°
PLATO J	24.5W	49.0N	1.03	1.00	0.92	0.77
LAPLACE D	25.5W	47.4N	1.00	1.00	0.97	0.79
PLATO M	15.5W	53.5N	1.05	1.00	0.93	0.77
ARISTILLUS FLOOR	1.2E	33.6W	0.95	1.00	0.94	0.88
ARISTILLUS RIM			0.98	1.00	0.89	0.80
ARISTILLUS HALO			0.93	1.00	0.97	0.91
PLATO RIM			0.84	1.00	0.92	0.83
ARISTARCHUS A	47.8W	25.9N	1.06	1.00	0.86	0.71
ARISTARCHUS FLOOR	47.5W	23.8N	0.86	1.00	0.83	0.74
ARISTARCHUS RIM			0.95	1.00	0.83	0.79
TENERIFE MTNS	13.0W	47.5N	0.99	1.00	0.95	0.77
MT PICO	9.0W	45.8N	0.99	1.00	0.92	0.72

TABLE I-2

IR, RADAR, AND OPTICAL SIGNATURES FOR TERRA UNITS IN THE PLATO STUDY AREA

	MONTES JURA — IRIDIUM FLANKS	PLATO'S HALO	MONTES ALPES	ARISTARCHUS PLATEAU
		UNIT		
LONG.	38-40	8-9W	4-6E	50-52W
LAT.	46-40N	54-56N	43-45N	26-28N
7.5m RADAR*	1.00	1.50	2.00	—
70cm RADAR*	1.00	0.50	1.00	0.50
3.8cm RADAR*	0.50	0.25	0.50	0.25
IR	0	0	2	TBD
3800A°	0.93±0.05	0.98±0.05	0.84±0.05	0.88±0.05
5600A°	1.00±0.05	1.00±0.12	1.00±0.06	1.00±0.13
8500A°	0.93±0.04	0.99±0.04	0.87±0.04	0.92±0.08
10500A°	0.89±0.05	0.93±0.02	0.81±0.02	0.94±0.03

* Average Mare = 1.00

TABLE I-3

OPTICAL SPECTRAL DATA
FOR MARE UNITS
IN THE PLATO STUDY AREA

UNIT	LON	LAT	3800A°	5600A°	8500A°	10500A°
PLATO FLOOR WEST	10-11W	51-52N	0.97	1.00	1.07	1.09
PLATO FLOOR EAST	8-9W	51-52N	1.01	1.00	1.09	1.19
MARE FRIGORIS	14-16W	56-58N	0.96	1.00	1.02	0.99
SINUS IRIDIUM FLOOR	32-34W	44-46N	0.92	1.00	1.01	1.04
IMBRIUM BLUE	22-24W	42-44N	1.03	1.00	0.99	1.00
IMBRIUM RED	12-14W	44-46N	0.94	1.00	0.99	0.98

```
MOON PLOT FOR  1 45 ON 12 16 1976

BEAM CO-ORDINATES - LONGITUDE(DEG)     20.000 LATITUDE     30.000

 MAP CO-ORDINATES - LONGITUDE(DEG)     6    30 LATITUDE    16    40

RADIUS OF PLOT(IN) 3.00


MAXIMUM DELAY(MS)  4.50

 LONG SUBRADAR POINT(DEG)       2.05
 LAT SUBRADAR POINT(DEG)        6.12

 DOPPLER ANGLE(DEG)              .60
 CENTER-LIMB FREQ DIFF(CPS)     6.40
 LIMB---LIMB FREQ DIFF(CPS)    12.80

 DELAY(SEC)                     2.646196
 MOON DIAMETER(MIN-ARC)        30.14


  BEAM CENTER
 DELAY RESOLUTION (KM) =  3.070
 FREQ. RESOLUTION (KM) =  2.814

 DELAY SEPARATION (MICROSEC)     10.000
 FREQ. SEPARATION (CPS)            .010

ACROSS BEAM
 MIN. DELAY (MILLISEC) =   .144
 MAX. DELAY (MILLISEC) =  4.966
 DELAY SPREAD(MILLISEC)=  4.822
 NO. OF DELAY BOXES   =  482
 FREQ. SPREAD  (CPS)  =  4.247
 NO. OF FREQ. BOXES   =  424



AT MAP CENTER
DELAY(MILLISEC) =  1.479
FREQ(CPS)       = -1.681
 NUM RANGE BOXES (MIN TO CENTER)  = 133
 NUM RANGE BOXES (CENTER TO MAX)  = 348
 NUM FREQ  BOXES (MIN TO CENTER)  = 212
 NUM FREQ  BOXES (CENTER TO MAX)  = 212
```

Table 3.1 Parameters for Radar Observations of Mare Serenitatis on 16 Dec. 1977, see Figure 3.1

```
MOON PLOT FOR  3 20 ON 12 18 1978

BEAM CO-ORDINATES - LONGITUDE(DEG)   -20.000 LATITUDE    52.000

 MAP CO-ORDINATES - LONGITUDE(DEG)  -50   10 LATITUDE   32   64

RADIUS OF PLOT(IN) 3.00


MAXIMUM DELAY(MS)  8.00

 LONG SUBRADAR POINT(DEG)      -.47
 LAT SUBRADAR POINT(DEG)       4.62

 DOPPLER ANGLE(DEG)            4.40
 CENTER-LIMB FREQ DIFF(CPS)    6.50
 LIMB---LIMB FREQ DIFF(CPS)   13.00

 DELAY(SEC)                    2.663132
 MOON DIAMETER(MIN-ARC)       29.95


  BEAM CENTER
 DELAY RESOLUTION (KM) =  1.956
 FREQ. RESOLUTION (KM) =  2.771

 DELAY SEPARATION (MICROSEC)    10.000
 FREQ. SEPARATION (CPS)           .010

ACROSS BEAM
 MIN. DELAY (MILLISEC) =  1.143
 MAX. DELAY (MILLISEC) = 11.595
 DELAY SPREAD(MILLISEC)= 10.452
 NO. OF DELAY BOXES  = 1045
 FREQ. SPREAD  (CPS)  =  4.341
 NO. OF FREQ. BOXES  =  434



AT MAP CENTER
DELAY(MILLISEC) =  4.153
FREQ(CPS)       =  1.702
 NUM RANGE BOXES (MIN TO CENTER)  = 301
 NUM RANGE BOXES (CENTER TO MAX)  = 744
 NUM FREQ  BOXES (MIN TO CENTER)  = 217
 NUM FREQ  BOXES (CENTER TO MAX)  = 217
```

Table 3.2 Parameters for Plato Radar Observations of 18 Dec. 1978, see Figure 3.1

	1969-1969 Mappings	Mare Serenitatis (16 Dec. 1979)	Plato (18 Dec. 1979)
Delay Resolution	10-40μsec	10μsec	10μsec
Surface Range Resolution (at Map Center)	5-10km	3.0km	2.0km
Spectral Resolution	0.02hz	0.01hz	0.005hz
Surface Frequency Resolution (at Map Center)	5-10km	2.8km	1.4km

TABLE 3.3 DIFFERENCES IN RADAR PARAMETERS BETWEEN NEW AND OLD RADAR OBSERVATIONS OF THE MOON.